Decay modes of high-lying single-particle states in ^{209}Pb

D. Beaumel,[1] S. Fortier,[1] S. Galès,[1] J. Guillot,[1] H. Langevin-Joliot,[1] H. Laurent,[1] J. M. Maison,[1] J. Vernotte,[1] J. A. Bordewijk,[2] S. Brandenburg,[2] A. Krasznahorkay,[2] G. M. Crawley,[3] C. P. Massolo,[4] and M. Rentería,[4]

[1]*Institut de Physique Nucléaire, Institut National de Physique Nucléaire et de Physique des Particles–Centre National de la Recherche Scientifique, 91406 Orsay Cedex, France*

[2]*Kernfysisch Versneller Instituut, 9747AA Groningen, The Netherlands*

[3]*National Superconducting Cyclotron Laboratory, Michigan State University, East Lansing, Michigan 48824*

[4]*Departamento de Física, Fac. Cs. Exactas, Universidad Nacional de La Plata, CC N° 67, 1900 La Plata, Argentina*

(Received 10 November 1993)

The neutron decay of high-lying single-particle states in ^{209}Pb excited by means of the (α,^{3}He) reaction has been investigated at 122 MeV incident energy using a multidetector array. The high-spin values of these states, inferred from previous inclusive experiments, are confirmed by the present data involving angular correlation measurements and the determination of branching ratios to low-lying levels in ^{208}Pb. The structure located between 8.5 and 12 MeV excitation energy in ^{209}Pb displays large departures from a pure statistical decay with significant direct feeding of the low-lying collective states (3^-,5^-) of ^{208}Pb. At higher excitation energy up to 20 MeV, the measured neutron decay is in agreement with the predictions of the statistical model.

PACS number(s): 21.10.Pc, 25.55.Hp, 21.10.Ma, 29.30.Hs

I. INTRODUCTION

Inclusive spectra of transfer reactions on medium and heavy nuclei show large giant resonancelike structures which correspond to the excitation of high-spin single-particle states far from the Fermi sea [1]. Such broad structures originate from the mixing of the initial single-particle mode with underlying complex states. The first step of this damping process is usually described as the coupling of the single-particle state with surface vibrations (particle-phonon coupling) [1,2]. In the following steps, coupling to more complicated configurations [3p-2h (three-particle–two-hole), 4p-3h, etc.] may occur until the system reaches a completely equilibrated stage, e.g., a compound nucleus.

Emission of a particle can occur at each stage of this damping process, as illustrated in Fig. 1. The total width Γ of the decaying state is usually written as the sum of two contributions $\Gamma^{\uparrow}$ and $\Gamma^{\downarrow}$, referred to as the "escape width" and the "spreading width," respectively. The escape width $\Gamma^{\uparrow}$ is related to the direct decay process, e.g., a fast nucleon emission either immediately after the primary excitation process or during the first steps of the damping process, as shown in Fig. 1. The spreading width $\Gamma^{\downarrow}$ is related to nucleon evaporation from the compound nucleus, whose corresponding decay channels can be predicted by statistical model calculations.

The investigation of the decay of high-lying single-particle giant states is an unique tool for studying the damping process, through the determination of the relative contributions of the "direct" and "statistical" decay modes. Information about the wave function of the state can be obtained when the observed decay differs significantly from statistical model predictions. In this case, one can determine the degree of thermalization of the mode $\Gamma^{\downarrow}/\Gamma$, and the direct branching ratios $\Gamma_i^{\uparrow}/\Gamma$, which measure the coupling to the ground and low-lying excited states of the target nucleus. These direct branching ratios can be compared with the predictions of microscopic nuclear models.

The present work is the first detailed study of the decay process for high-lying, high-spin single-particle states. We report here the results obtained for the decay modes of ^{209}Pb states excited by means of the one-neutron transfer (α,^{3}He) reaction at 122 MeV. A large bump located at $E_x \simeq 10$ MeV in this nucleus has been observed in the inclusive spectra of (α,^{3}He) [3], (^{20}Ne,^{19}Ne) [4,5], and (^{40}Ar,^{39}Ar) [5] reactions at incident energies around (30–50)A MeV. The excitation energy, angular distribution,

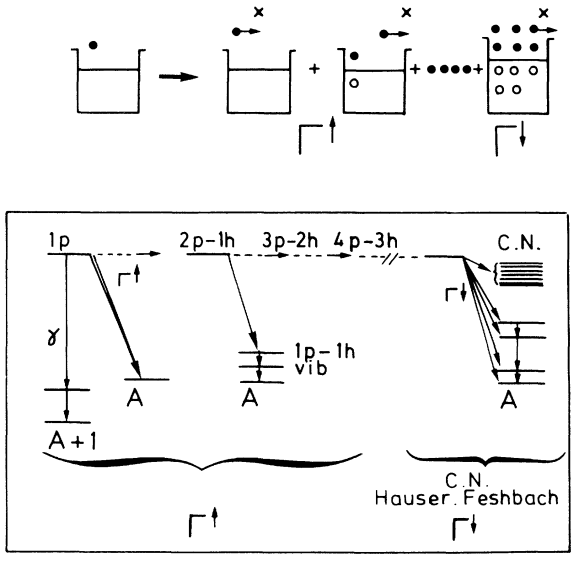

FIG. 1. Schematic representation of the decay process of a high-lying single-particle state.

and strength of this structure, as well as the comparison with theoretical predictions [1,2], strongly suggest that it arises from neutron stripping to the available high-spin outer subshells, i.e., $2h_{11/2}$,$1j_{13/2}$, and $1k_{17/2}$.

The experiment has been performed using the neutron multidetector EDEN [6], built at IPN Orsay in collaboration with physicists from KVI Groningen, in order to measure neutron decay channels with high statistics and good energy resolution. The experimental setup and the procedure for the data reduction are described in the next section. Qualitative results of the decay experiment may be readily obtained by observing the main features of inclusive and exclusive spectra, which are reported in Sec. III. The method of analysis used to extract quantitative information is summarized in Sec. IV. This section contains the formalism for predicting the angular correlations, which is needed to determine branching ratios and obtain information about spin values, and describes the statistical model calculations which predict the characteristics expected for a pure statistical decay. The dependence of the decay properties of the ^{209}Pb continuum states on excitation energy and the corresponding direct branching ratios $\Gamma_i^{\uparrow}/\Gamma$ for the various neutron decay channels (ground state, 3^-, 5^-, etc.) will be discussed in Sec. V.

II. EXPERIMENTAL PROCEDURE

The ^{208}Pb(α,^{3}He n)reaction has been investigated using an α-particle beam of 122 MeV delivered by the KVI AVF cyclotron. The thickness of the 99.9% isotopically enriched ^{208}Pb target was 6.8 mg/cm^2. The outgoing ^{3}He particles emitted in a solid angle of 10 msr around 0° were detected at the focal plane of the QMG/2 magnetic spectrograph [7], using a multiwire drift chamber [8] backed by a plastic scintillator. The direct beam was stopped in a Faraday cup placed between the first and second dipole magnets. The position and angle information given by the multiwire detector, added to time of flight and energy loss measurements provided by the plastic detector, permitted a good identification of ^{3}He particles originating from the target. Excitation energies in ^{209}Pb between 3.9 MeV, the threshold energy for one neutron emission, and 22 MeV could be investigated with a single setting of the magnetic field. The energy calibration of the focal plane was determined by measuring the position of ^{3}He peaks corresponding to ^{13}C and ^{17}O levels with accurately known energy, excited by the (α,^{3}He) reaction on a mylar target.

A detailed description of the EDEN neutron multidetector array and of its performances has been given in Ref. [6]. It consists of 40 cylindrical cells, with a diameter of 20 cm and a thickness of 5 cm, filled with the NE213 liquid scintillator, which gives good discrimination between neutrons and γ rays. They were placed at 1.75 m from the target position. Fifteen detectors were put in the horizontal plane, on both sides of the incoming beam, from 68° to 168° and from 190° to 208°, with a spacing of about 9°. The remaining detectors were arranged in two shells above and below the horizontal plane at azimuthal angles of ±9°.

In addition a Ge(Li) detector was placed at 90° in order to detect the γ rays emitted either by the primary ^{209}Pb nucleus or by ^{208}Pb and ^{207}Pb after emission of one and two neutrons, respectively. Its efficiency at 25 cm from the target was about 0.4×10^{-3}.

The energy of the neutrons was deduced from a time of flight measurement, with the stop signal being provided by the RF signal of the cyclotron. Instabilities in the arrival of the beam burst on target with respect to the RF signal were accounted for by checking the position of the time peak corresponding to prompt γ rays. The energy resolution ranges from 60 keV at 1 MeV to 500 keV at 6 MeV, as determined [6] by the calibration measurement with a Mylar target.

In order to extract quantitative information from the data, it is necessary to know accurately the absolute intrinsic efficiency ϵ of each individual neutron detector as a function of neutron energy E_n. The intrinsic efficiency of one cell for E_n between 0.5 and 6 MeV was determined experimentally by measuring neutrons emitted from a ^{252}Cf source in coincidence with fission fragments, for various thresholds on the energy deposited in the scintillator [6]. The dependence of efficiency versus neutron energy above 0.5 MeV was parametrized in the form $\sum_{i=1}^{6} a_i/E_n^i (i = 1,6)$, the a_i coefficients being obtained from a fit to the data. The results are in very good agreement with those of Monte Carlo calculations for neutron energies above 2 MeV, whereas the experimental efficiency is about 10% higher than the predicted one at lower energies, as discussed in Ref. [6]. For the 60 keV electron-equivalent energy threshold, used in the present analysis, the absolute intrinsic efficiency of one NE213 cell ranges between 30% and 55% in the 0.5–6 MeV neutron energy range, ensuring an overall efficiency (including the total solid angle) of the multidetector $\epsilon\Omega_T/4\pi$ slightly above 1%.

The efficiencies $\epsilon(E_n)\Omega/4\pi$ are expected to be identical for each individual detector due to the geometrical arrangement, provided that electronic fluctuations inducing some uncertainty on the effective threshold values are negligible. This was checked in a preliminary experiment by counting neutrons emitted by an Am-Be source placed at the target position. The start signal of the time of flight measurement was given by the 4.43 MeV γ ray from the reaction ^{7}Be(α,n)^{12}C. The average fluctuations of relative efficiencies $\Delta\epsilon/\epsilon$ versus the mean values were found to be about 7% for neutron energies above 1 MeV and 15% for the 0.5–1 MeV energy range. Special care was taken to check the calibration of each detector at different stages of the experiment, using ^{241}Am and ^{137}Cs γ-ray sources. Only neutrons with energy above 0.5 MeV were considered in the analysis, due to the large uncertainty in the efficiency at lower energies.

Multiparameter events corresponding to a coincidence between the focal plane plastic scintillator and the EDEN or Ge(Li) detectors were registered on magnetic tape, together with scaled-down single events for absolute normalization of coincident data. The 600 ns width of the coincidence window allowed us to simultaneously record random events for subsequent subtraction. In the typical conditions of the experiment (about 5000 counts/s in one

EDEN cell and 8000 counts/s in the focal plane detector for 0.5 nA beam), the ratio of true to random coincident events was about 1.2.

Two-dimensional true+random and random [$E_{^3\mathrm{He}} - E_n$] energy spectra obtained for each detector have been corrected for efficiency effects. They were further transformed into [$E_{x_a} - E_{x_b}$] spectra, where E_{x_a} is the excitation energy in ^{209}Pb and E_{x_b} is defined by the following expression:

$$E_{x_b} = E_{x_a} - E_n(\mathrm{c.m.}) - S_n, \quad (1)$$

S_n being the one-neutron emission threshold (3.94 MeV).

In the case of one-neutron emission, E_{x_b} is the excitation energy of the final level in ^{208}Pb fed by the neutron decay. Above the two-neutron emission threshold, a spectrum displayed as a function of E_{x_b} corresponds to the sum of neutrons from decay to ^{208}Pb states and neutrons emitted from subsequent decay to ^{207}Pb. On the other hand, only rather low statistics could be obtained for these triple-concident (^{3}He-n-n) events, as shown in Sec. V. Data were finally extracted from projected E_{x_a} and E_{x_b} spectra, obtained after subtraction of random events. The widths of the energy bins were chosen in order to get sufficient statistical accuracy for the data. In particular, angular correlations were measured for variable bins of ^{209}Pb excitation energy ranging from 0.5 MeV to 4 MeV, after summation of two or three detectors at the same angle. On the other hand, 0.2 MeV energy bins were used for the extraction of branching ratios, as shown below.

Qualitative results can be readily obtained by considering E_{x_a} and E_{x_b} projected coincident spectra, summed over all the detectors for the whole energy range under study. They will be shown in the next section, together with the inclusive ^{3}He spectrum. In addition, we will present ^{3}He spectra in coincidence with γ rays observed in the EDEN detectors and in the Ge(Li) detector.

III. INCLUSIVE AND EXCLUSIVE SPECTRA

A. (α,^{3}He) singles events

The (α,^{3}He) spectrum observed for singles events is shown in Fig. 2(a). It is dominated by a large asymmetric bump located in the 8.5–12 MeV region with a maximum at approximately 10 MeV. Narrow peaks can be observed below 8.5 MeV, superimposed on a slowly rising continuum, whereas the region above 12 MeV displays a monotonic decrease of the cross section with energy. Above 20 MeV, the spectrum is dominated by a large peak [not displayed in Fig. 2(a)] due to hydrogen contamination of the target. On the other hand, carbon and oxygen contaminants [labeled with c in Fig. 2(a)] only make quite small contributions to the ^{3}He spectrum at excitation energies above 4.5 MeV.

In the previous experiment performed at 183 MeV [3], the giant resonancelike structure observed around 10 MeV was embedded in a large continuum rising with excitation energy. The origin of this continuum was attributed to three-body events such as the breakup of the incident α particle. This underlying background appears to be considerably reduced in the inclusive spectrum at 122 MeV. The determination of the centroid energy E and full width at half maximum (FWMH) essentially depends on the amount of the continuum which is subtracted. Assuming a straight line like the one displayed in Fig. 2(a), we obtain E=9.7 MeV, FWMH of 2.6 MeV. Using other different reasonable assumptions for the background leads to an estimate of the uncertainty on both values of about 0.3 MeV. These characteristics are consistent with the previous results [3].

B. (α,^{3}He) coincident events

The general features of the ^{3}He spectrum of Fig. 2(b), measured in coincidence with neutrons, are quite dif-

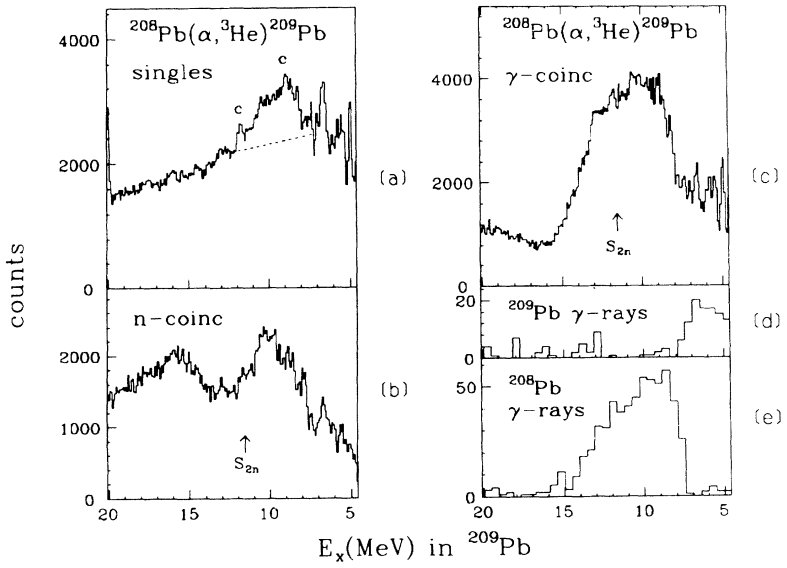

FIG. 2. ^{208}Pb(α,^{3}He)^{209}Pb spectra at $\theta_{^3He} = 0°$: (a) singles spectrum; (b) coincidence with neutrons detected by EDEN; (c) coincidence with γ rays detected by EDEN; (d) coincidence with the 779 keV or 1423 keV γ rays from ^{209}Pb, detected by the Ge(Li) counter; (e) coincidence with the 583 keV or 2613 keV γ rays from ^{208}Pb, detected by the Ge(Li) counter.

ferent from those observed in the inclusive spectrum of Fig. 2(a). In particular, the position of the maximum of the 10 MeV structure appears shifted upwards by about 1 MeV and some peaks observed at low excitation energy in the singles spectrum are missing. Moreover, a second bump is observed around 16 MeV, where the inclusive spectrum displays a structureless continuum. It will be shown in Sec. V that such behavior originates from the competition between the γ, n, and $2n$ decay channels. This may be qualitatively understood by considering the (α,^{3}He) spectra in concidence with γ rays.

The spectrum of ^{3}He events in coincidence with all γ rays detected by EDEN is shown in Fig. 2(c). In the low-energy part, it displays narrow peaks which are not observed in the neutron-coincident spectrum of Fig. 2(b). Additional information about the origin of the emitted γ rays can be obtained by studying the ^{3}He events in coincidence with γ rays detected by the Ge(Li) counter. With the 3 keV energy resolution of this detector, some γ rays can be readily identified with well-known transitions in ^{209}Pb and ^{208}Pb , although the low statistics of the Ge(Li) data does not allow the identification of all the γ rays emitted in the decay cascade. In particular the 779 keV and 1423 keV secondary transitions are clearly observed in coincidence with ^{3}He particles in the region below 8 MeV excitation energy. These γ rays correspond to the ground state decay of the low-lying $1i_{11/2}$ and $1j_{15/2}$ particle states in ^{209}Pb. The ^{3}He spectrum in coincidence with at least one of these two ^{209}Pb transitions is displayed in Fig. 2(d). It is therefore evident that a competition between neutron decay and gamma decay exists in a large region above the neutron emission threshold of 3.9 MeV, producing the observed distortion in the exclusive spectrum in coincidence with neutrons. This inhibition of neutron emission up to 4 MeV above the threshold can only be explained by the effect of the centrifugal barrier for neutrons with large angular momentum. The narrow peaks observed in Figs. 2(a) and 2(c) may then be interpreted as due to the excitation of levels with high-spin values, for which neutron decay is heavily hindered due to low penetrabilities.

A large bump is observed between 8 and 15 MeV in the ^{3}He spectrum of Fig. 2(c), coincident with all the γ rays detected by EDEN. In this region, the Ge(Li) spectra displays strong lines at 2613 keV and 583 keV, related to the γ decay of the lowest 3^- and 5^- states in ^{208}Pb, which are fed either directly by the neutron decay or by γ rays originating from higher-lying levels. The corresponding ^{3}He spectrum associated with one-neutron decay to ^{208}Pb is shown in Fig. 2(e), which displays the same 8–15 MeV bump as in Fig. 2(c). Therefore, one observes one-neutron decay followed by γ emission in a large region above the two-neutron emission threshold of 11.3 MeV, whereas the two-neutron emission process is predominant only above 15 MeV. On the other hand, only a very low rate of γ emission from ^{207}Pb is associated with two-neutron emission below this energy, due mainly to the feeding of the ground state and of the $J^\pi=13/2^+$ isomer at 1.633 MeV. It will be shown in Sec. V that the second bump centered at 16 MeV in the neutron-coincident spectrum of Fig. 2(b) corresponds to the slow rise of the neutron multiplicity from the two-neutron threshold to this energy.

C. Total neutron decay spectrum

The neutron spectrum from the decay of the 4–20 MeV energy bin in ^{209}Pb, summed over all EDEN detectors, is displayed in Fig. 3 as a function of the final energy E_{x_b}. Transitions to discrete states in ^{208}Pb are observed as sharp peaks. One observes a strong excitation of the ground state and the low-lying collective states at 2.61 MeV ($J^\pi=3^-$) and 3.20 MeV ($J^\pi=5^-$). Excitation of the 4^- level at 3.47 MeV and of the second 5^- level at 3.71 MeV can be observed in the summed spectrum, although it is not possible to extract detailed information about the population of these levels. Using a peak decomposition procedure, one can estimate that these two levels only contribute to about 15% to the neutron peaks at 3.2 MeV and 4.0 MeV, respectively.

From the peak decomposition analysis, one may deduce that the main contribution to the peak observed around 4 MeV is due to the neutron decay to the 7^- level at 4.03 MeV. The 8^+ level at 4.61 MeV is also clearly populated. The broad peak centered at 4.9 MeV excitation energy is an unresolved multiplet of states, with a shape consistent with a strong population of the next yrast 10^+ level at 4.89 MeV. The interpretation of the bump observed at about 10 MeV in ^{208}Pb is not straightforward, as the E_{x_b} spectrum above the 7.4 MeV neutron emission threshold may result from the addition of the primary neutron spectrum to the one corresponding to a second neutron emitted by a high-lying excited state in ^{208}Pb. This will be discussed in Sec. V.

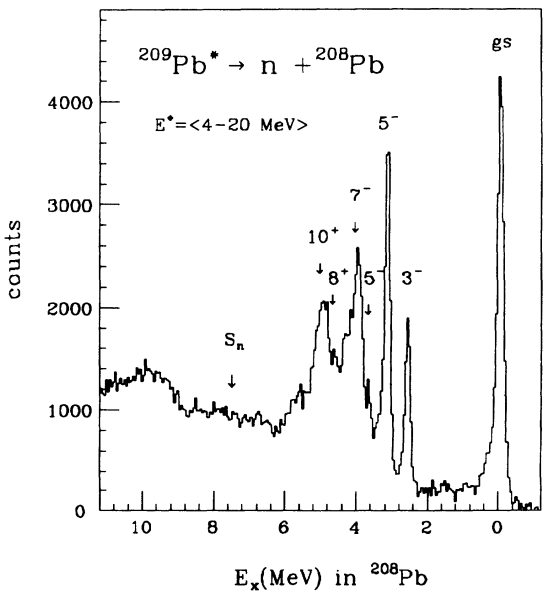

FIG. 3. Population of final states in ^{208}Pb from the neutron decay of ^{209}Pb between 4 and 20 MeV excitation energy.

IV. DATA ANALYSIS

The analysis of angular correlation data provides quantitative results about experimental branching ratios and also may give some information about the spin values of the emitting states, as shown in Sec. IV A. In a second step, one has to estimate the contribution of statistical decay to the data in order to extract direct branching ratios $\Gamma_i^{\uparrow}/\Gamma$, which can be compared with the predictions of microscopic models. The procedure which has been adopted and the resulting ingredients of the statistical model calculations are described in Sec. IV B.

A. Angular correlation analysis

1. *Theoretical angular correlations deduced from DWBA calculations*

In an axially symmetric system, the angular correlation for the decay of an initial state of spin J_a to a final state J_b can be written [9–11]

$$W(\theta) = (2J_a+1)^{\frac{1}{2}} \sum_k \sum_{M_a} \langle J_a J_a M_a - M_a | k0 \rangle P(M_a) F_k(a,b) Q_k P_k(\cos\theta) \ . \tag{2}$$

The density matrix elements $P(M_a)$, giving the relative population of its magnetic substates M_a, contain all information about the alignment of the emitting state. The spin dependence of the correlation is given by the $F_k(a,b)$ coefficients, which are linear combinations of geometrical recoupling coefficients and depend on the interference of the partial waves (l,j) involved in the decay process [11]. The sum of Legendre polynomials is limited to even values of k with

$$k_{\max} = \min[2J_a, \max(2l), \max(2j)] \ . \tag{3}$$

In the particular case of neutron decay to the 0^+ ground state, only one partial wave exists so that F_k only depends on the spin value of the initial state. The attenuation of the angular correlation due to the finite size of the neutron detectors is accounted for by the Q_k coefficients, which are calculated using the procedure of Ref. [12].

In the $(\alpha,{}^3\mathrm{He})$ reaction on a target with zero spin, considering the spin value of the incoming and outcoming particles, only the magnetic substates $M_a = \pm 1/2$ can be populated at 0°. However, due to the 3° opening angle of the spectrometer, the population of other magnetic substates is different from zero. The $P(M_a)$ values can be deduced [13] from the reaction amplitudes $\beta_{M_a}(\theta_{^3\mathrm{He}})$ calculated for the excitation process, by averaging the quantity $\beta_{M_a}(\theta_{^3\mathrm{He}})\beta^*_{M_a}(\theta_{^3\mathrm{He}})/\sum_{M_a}|\beta_{M_a}(\theta_{^3\mathrm{He}})|^2$ over the solid angle.

The reaction amplitudes have been calculated using the code DWUCK4 [14], which assumes that the emitting nucleus has been populated via a direct transfer to a resonant state with spin J_a, using the distorted wave Born approximation (DWBA) formalism. Stripping to unbound states is calculated using the Vincent and Fortune method [15].The optical potential parameters in the entrance and exit channels were those used in the DWBA analysis [3] of the same reaction at 183 MeV. Standard parameters r_0=1.25 fm, a=0.65 fm, and λ=25 were used for the neutron form factor. Calculations performed at 122 MeV incident energy predict the same preferential excitation of high-spin single-particle states as at 183 MeV, with the cross section increasing with spin value. Cross sections at forward angles are expected to be 4–5 times larger for $1k_{17/2}$ states than for $1j_{13/2}$ states, at equal spectroscopic strengths. Moreover, the ratio of theoretical cross sections for $1k_{17/2}$ and $2h_{11/2}$ transitions is found to vary from 6 to 40 between 6 and 10 MeV excitation energy.

Averaged density matrices and the resulting theoretical angular correlations have been calculated using the particle-particle angular correlation code CORELY [13] for various assumptions of initial spin values and nlj transfer. The values of $P(\pm 1/2)$ are typically about 70% for $J_a \geq 7/2$ states, with the remaining strength strongly concentrated in the magnetic substates $M_a = \pm 3/2$. These values were found to be weakly dependent on the excitation energy. Additional DWBA calculations with other reasonable sets of optical parameters [16] were found to give similar results.

Shapes of the angular correlations for ground state transitions are displayed in Fig. 4. The maximum neutron yield is obtained at 180°. For opening angles of both the spectrometer and neutron counters equal to zero, the theoretical value of $W(180°)$ would be J_a+1/2. In the present experimental conditions, the global attenuation

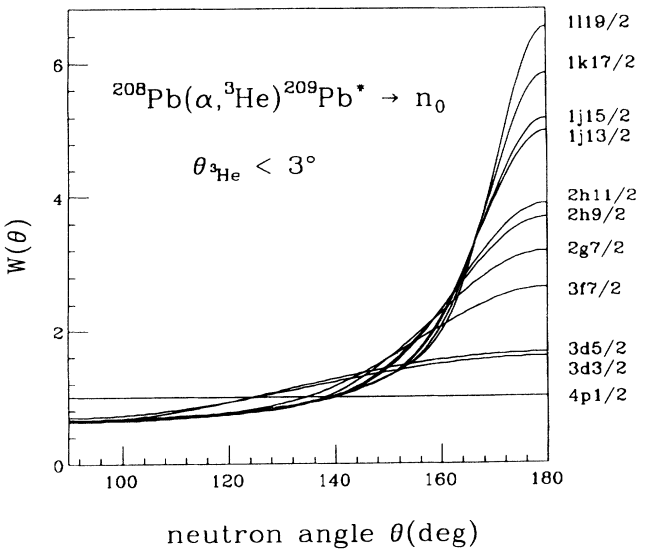

FIG. 4. Neutron angular correlations calculated for the ground state decay of an initial state in ^{209}Pb populated by a nlj direct transfer.

of neutron yield at 180° is about 30%, as shown in Fig. 4. It appears clearly that spin determination through angular correlation measurements strongly depends on the backward angle data.

Similar backward enhancements of neutron yields have also been calculated for transitions to excited states, in the particular case where only one partial wave (l,j) with the minimum value $|J_a - J_b|$ is involved in the decay. This limitation to one main partial wave is a good approximation in the case of low-energy neutrons, for which the centrifugal barrier inhibits the emission of partial waves with higher j values. Otherwise, calculations for transitions to final levels with $J_b \neq 0$ require a detailed knowledge of the wave function of the emitting state, in order to account for interference terms in the F_k coefficient of Eq. (2).

2. Determination of experimental branching ratios

The present analysis of the angular correlation $W(\theta)$ of neutrons emitted from an energy bin in the $(\alpha,{}^3\mathrm{He})$ continuum implicitely assumes that they result from the sequential decay of several states with different possible spin values, without parity mixing. In such a case, the angular correlation is given by the addition of the individual contributions as expressed in Eq. (2). The number of counts $N_{a\to b}(\theta)$ corresponding to the neutron decay of an energy bin around E_{x_a} in ^{209}Pb, to various final levels E_{x_b} in ^{208}Pb, extracted for each EDEN detector or group of detectors, may be expressed by the following expression:

$$N_{a\to b}(\theta) = \sum_k A_k P_k(\cos\theta) = A_0 W(\theta) \ . \qquad (4)$$

The sum runs over even values of k, with a limitation on $k_{\max}$ depending on spin and orbital angular momenta according to Eq. (3).

The angular correlation is therefore expected to be symmetric with respect to 90° (c.m.). The origins of possible asymmetries in the correlation may arise from interferences between the contributions of several overlapping ^{209}Pb states with different parities or the presence of a significant contribution of breakup processes to the $(\alpha,{}^3\mathrm{He}\,n)$ cross section. The most forward laboratory angle of the experimental correlation is 68°, which allows us to test if these contributions may be reasonably neglected.

From the A_0 normalization coefficient of the correlation, one can deduce the experimental value of the branching ratio $B_{a\to b}$ for the $a \to b$ transition using the expression

$$B_{a\to b} = A_0 (N_s \epsilon \Omega/4\pi)^{-1} \ , \qquad (5)$$

where $\epsilon\Omega/4\pi$ is the global efficiency of an individual counter and N_s is the number of corresponding events observed in the singles spectrum.

Branching ratios $B_{a\to b}$ and the angular correlation function $W(\theta)$ have then be determined by a least squares fitting procedure, minimizing the quantity

$$\chi^2 = (1/n) \sum_j [N_{a\to b}(\theta_j) - A_0 W(\theta_j)]^2/\sigma_j^2 \ , \qquad (6)$$

where n is the number of degrees of freedom for the fit and σ_j is the uncertainty assigned to the neutron yield at angle θ_j. This was done for all values of the maximum order of the Legendre polynomial series up to $k_{\max}$=16. The adopted value of $B_{a\to b}$ was the one corresponding to the value $k_{\max} = k_M$ giving the lowest value of χ^2. Within the error bars, the value of $B_{a\to b}$ was found to be nearly independent of the value of $k_{\max}$.

In the case of one-neutron emission to a level or group of levels in ^{208}Pb, the branching ratio $B_{a\to b}$ should be identical to the ratio of the partial neutron width to the total width $\Gamma_{a\to b}/\Gamma$, provided that the neutron energy is larger than 0.5 MeV and that the total $(\alpha,{}^3\mathrm{He})$ cross section in the singles spectrum corresponds to excitation in ^{209}Pb. If this is not the case, in particular when an underlying background is present in the inclusive spectra, the $\Gamma_{a\to b}/\Gamma$ branching ratio will be underestimated by the present analysis. The results will be shown in the next section.

Angular correlations $W(\theta)$ determined for transitions to the ground state have been compared to the theoretical functions displayed in Fig. 4 for different spin values of the emitting states in ^{209}Pb, in order to determine if one of these states are predominant in the excitation energy range. In the case of transitions to the 3^- and 5^- states, the experimental correlations have been compared to functions calculated for different J_a values according to Eq. (2), using the simplifying assumption of only one (l,j) partial wave contributing to the decay. A possible emission by two states with different spin values has also been accounted for by fitting a weighted sums of the corresponding angular correlations to the data. The results of the angular correlation analysis, in terms of spin assignments and branching ratios will be discussed in Sec. V.

B. Determination of the statistical contribution

1. Direct branching ratio extraction procedure

Once the experimental decay properties of continuum states in ^{209}Pb have been established, one must examine whether the results are consistent with the assumption of decay of a completely equilibrated compound nucleus. In such a case, the branching ratios for the population of the different final states are fully determined by spin distributions in the compound nucleus, level densities in the residual nuclei, and transmission coefficients, and can in principle be predicted by the statistical model. One has to investigate the sensitivity of the statistical model calculations to these more or less firmly established parameters to determine if some reasonable choice of input parameters reproduces the measured decay branching ratios in a satisfactory way. This can be done by comparing the experimental neutron spectra, corrected for detector efficiency, to the calculated spectra folded with the energy-dependent resolution, after suppression

of neutron energies below the 0.5 MeV threshold.

If these attempts to predict the data by statistical calculations are unsuccessful, one may conclude that there is evidence for an additional contribution to the decay, namely, the direct decay. The fraction F of inclusive cross section decaying by statistical emission, namely, the degree of thermalization of the system, may be estimated by normalizing the calculated neutron spectrum (where the number of decaying nuclei is given by the number of counts in the inclusive spectrum) to the experimental one. This normalization is usually done by superimposing the low-energy neutron regions of both spectra, with the condition that the statistical spectrum does not exceed the experimental one anywhere.

High-energy neutrons observed in excess of the normalized statistical spectra are assumed to originate from the direct emission process. The contribution of the statistical decay process to the measured branching ratio is taken as the product of the factor F by the branching ratio $(\Gamma_i/\Gamma)_{\rm calc}$ calculated using the statistical model. The direct branching ratios may be therefore extracted using the relation:

$$\Gamma_i^{\uparrow}/\Gamma = (\Gamma_i/\Gamma)_{\rm expt} - F(\Gamma_i/\Gamma)_{\rm calc} \,. \qquad (7)$$

2. *Statistical decay calculations*

The calculations have been performed using the code CASCADE [17], based on the Hauser-Feshbach formalism. The sensitivity to input data, i.e., transmission coefficients for the emitted neutrons, dominant spin values in the emitting compound nucleus, and level densities in the residual nuclei, is discussed below.

a. Transmission coefficients. Transmission coefficients for neutrons have been evaluated using the optical potential from Wilmore and Hodgson [18]. The use of a different set of optical potential parameters (Rapaport *et al.* [19]) leads to only small differences in the final results. In particular statistical branching ratios to the 3^- and 5^- states calculated for neutrons emitted from the 8–12 MeV structure were found to differ by less than 15% using these two different assumptions.

b. Distributions of spin values in the compound nucleus. The second important input data are the distributions of initial spins in ^{209}Pb as a function of excitation energy. Information on the distribution of single-particle strengths between 6 and 12 MeV excitation energies in ^{209}Pb have been obtained previously from a DWBA analysis [3] of the ^{208}Pb(α,^{3}He)^{209}Pb at 183 MeV, showing mixing of L = 5, 7, and 8 angular momentum transfer. The results of this analysis have been used as a starting point for the statistical model calculations. An example of the dependence of the calculated statistical decay spectra on different assumptions for the initial spin distribution will be shown in Sec. V. The adopted spin distributions, giving the best agreement between the calculated and experimental decay properties—i.e., the relative population of the final states in ^{208}Pb and the neutron multiplicity—are displayed in Fig. 5. In particular, the decay results between 9 and 12 MeV are consistent

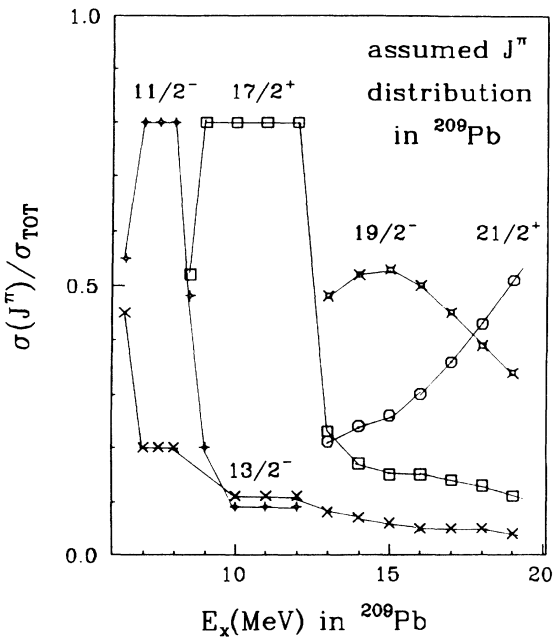

FIG. 5. Spin distribution of initial ^{209}Pb states, which have been used as input for the statistical calculations leading to the extraction of direct $\Gamma^{\uparrow}/\Gamma$ branching ratios (see text).

with a predominant excitation of $17/2^+$ states, which is in agreement with the DWBA results of Ref. [3].

Above 12 MeV excitation energy in ^{209}Pb, the measured ratio of two-neutron over one-neutron decay can only be reproduced by the calculations with high-spin initial states as input data, in agreement with the known selectivity of the (α,^{3}He) reaction for transferring high angular momenta. In this region, we have used the predictions [20] of the Bonaccorso-Brink model [21] which describes stripping reactions to continuum states. From this calculation, the inclusive (α,^{3}He) spectrum results from the addition of different L contributions, with L = 8, 9, and 10 waves being predominant in this energy range. The additional assumption J_i=L+1/2 was made in order to obtain the spin distributions shown in Fig. 5 for energies above 12 MeV.

c. Level densities. From a practical point of view, the CASCADE code has the crucial advantage of allowing the inclusion of a number of discrete states in the level densities . All the experimentally known discrete states up to around 5 MeV in ^{208}Pb, 3.5 MeV for ^{207}Pb, and a few MeV for the neighboring nuclei have been included. At higher energy, level densities are parametrized using the analytic form of the backshifted Fermi gas model. The main parameters [17] are the term a, giving the energy dependence of the density, the pairing energy Δ, and the effective moment of inertia I. In the energy region just above the highest discrete levels and below an energy E_1 (commonly chosen equal to $60A^{-1/3}$ MeV), these parameters are those empirically determined by Dilg *et al.* [22]. At very high excitation energy (above E_2 = $120A^{-1/3}$ MeV), these parameters are those predicted by the liquid drop model [17]. Between these two regions, a linear interpolation of these parameters as a function of the ex-

citation energy is made by the code.

It can be noticed that the statistical decay of the high-spin states excited by the (α,^{3}He) reaction predominantly populates high-spin states in ^{208}Pb and that the extrapolation of the Dilg parametrization obtained for low-spin levels may be questionable. Some minor adjustments of the density parameters used in the code have therefore been made in order to avoid discontinuities at the borders of the energy regions defined above. The results of these adjustments are shown in Fig. 6 for narrow energy slices at 16.5, 13.5, and 10.5 MeV in ^{209}Pb.

At 13.5 MeV, the exponential part of the neutron spectrum corresponds to decay to the 5–8.5 MeV excitation energy region in ^{208}Pb. Statistical calculations using Dilg density parameters for this region do not predict the correct energy dependence of the neutron spectrum [dotted line in Fig. 6(b)]. Much better agreement is obtained by changing the interpolation region $[E_1 - E_2]$ from [10–20 MeV] to [6–12 MeV], thus increasing the ^{208}Pb level density used in the calculation. An additional adjustment has to be made in order to avoid the discontinuity between the region of discrete levels and the low-energy part of the calculated level density in ^{208}Pb. This was achieved by multiplying the calculated density by a factor N, this factor varying linearly between 0.6 at 5 MeV and 1 at 10 MeV. The effect of these adjustments on the calculated spectra are shown as solid lines in Figs. 6(b) and 6(c).

A similar adjustment of the parametrized level density in ^{207}Pb has to be made in order to reproduce the neutron spectrum from the decay of ^{209}Pb at higher excitation energies where two-neutron emission is predominant. This was done by adopting the liquid drop model expectation value of the a parameter above 3.5 MeV excitation energy in ^{207}Pb, and fixing the $[E_1 - E_2]$ interpolation region for the I and Δ parameters to [3.5–9.5 MeV]. Figure 6(a) compares the experimental neutron spectrum at 16.5 MeV excitation energy with the results of statistical calculations, using standard (dotted line) and adjusted (solid line) level density parameters. The data are well reproduced by the adjusted parameters, which correspond to a level density in ^{207}Pb higher than the one predicted by the parametrization of Ref. [22].

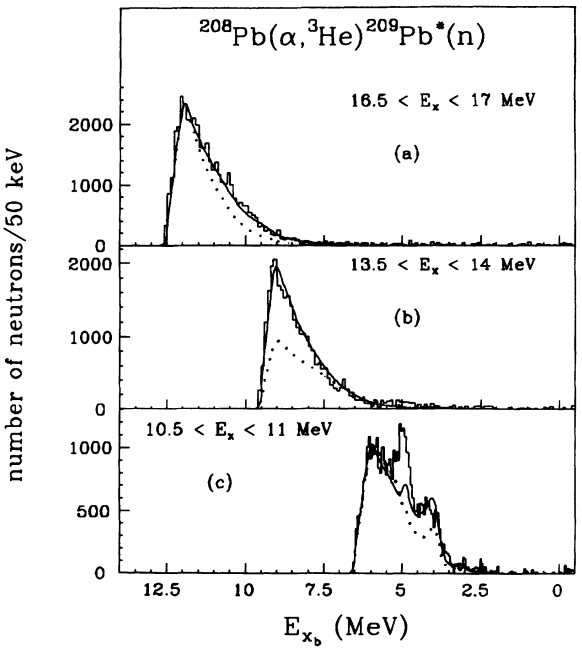

FIG. 6. Experimental neutron spectra, displayed as function of final ^{208}Pb excitation energy and corrected for detector efficiency, for three 0.5 MeV wide energy bins in ^{209}Pb. They are compared with statistical spectra, calculated using the assumptions reported in the text and convoluted with the resolution of the detectors. For the 10.5 and 13 MeV slices, the dotted line corresponds to calculations performed using a standard ^{208}Pb level density (see text).

V. RESULTS AND DISCUSSION

The inclusive and exclusive ^{3}He spectra of Fig. 2 may be divided into three different parts: the low-energy region below 8.5 MeV, where there exists a competition between neutron and γ-ray emission, the region of the bump up to about 12 MeV, and the continuum above. The experimental results obtained in these three regions are reported in Sec. V A and compared with the predictions of statistical decay calculations. Section V B will be particularly devoted to the results concerning the extraction of direct branching ratios in the bump region, which can be compared with the detailed predictions of the available microscopic nuclear models.

A. Branching ratios, spin assignments, and comparison with statistical calculations

Neutron branching ratios $B_{a\to b}$ corresponding to decay to levels or groups of levels in ^{208}Pb and to higher-energy bins in the spectrum of Fig. 3 have been systematically determined for each 200 keV energy bin between 4.5 MeV and 20 MeV excitation in ^{209}Pb. The energy dependence of the branching ratios is plotted in Fig. 7 for the transi-

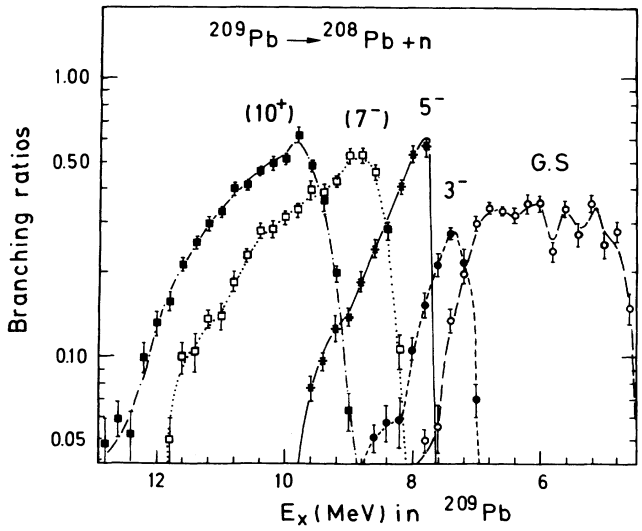

FIG. 7. Branching ratios Γ_n/Γ of transitions to the ^{208}Pb ground state and excited levels or group of levels.

tions to the ^{208}Pb ground and excited states, e.g., 3^- at 2.61 MeV, 5^- at 3.20 MeV (including a weak contribution of the 4^- level at 3.47 MeV), and groups of high-spin levels at 4.0 and 4.9 MeV.

The ground state branching ratio is found to be approximately constant from 4.8 MeV to 7 MeV. These two energies correspond to the threshold for neutron decay to the ground and 3^- states, respectively, with a 0.8 MeV shift probably due to centrifugal barrier effects. Above 7 MeV, the ground state branching ratio drops very quickly below 10%. Branching ratios for excited states display a similar behavior with increasing excitation energy, e.g., a sharp rise just above their own emission threshold, and then a rapid decrease above the threshold for the decay to the next populated state at higher energy. A qualitative explanation to this abrupt change at the opening of each new neutron channel, implying more and more large spin values of the final state $(0^+, 3^-, 5^-, 7^-, 8^+, ...)$, is readily obtained by considering the high-spin values of the initial state and the large differences of transmission coefficients for low-energy neutrons with different angular momenta.

The sum of the partial branching ratios $B_{a\to b}$ is the multiplicity of neutrons with energies above 0.5 MeV. The dependence of the experimental multiplicity on excitation energy of ^{209}Pb states is shown in Fig. 8. The relative uncertainty on the multiplicity is estimated to be about 15%, due to the combination of statistical errors on branching ratios and systematic uncertainties in the absolute efficiencies of the neutron detectors. The predictions of statistical calculations for the multiplicity of neutrons with energy above 0.5 MeV are plotted for comparison. They will be discussed below.

1. *Low-lying unbound states in ^{209}Pb: 5 MeV $\leq E_x \leq$ 8.5 MeV*

Neutron angular correlations measured in this energy region are displayed in Fig. 9. Angular correlations for the ground state transition are presented for three energy bins in the ^{209}Pb excitation energy spectrum of Fig. 2(b), e.g., the structure observed around 6.6 MeV, and adjacent lower- ($E_x \leq 6.2$ MeV) and higher- (7 MeV $\leq E_x \leq$ 8 MeV) energy bins. Figure 9 also displays the angular correlations measured in the region below 8.5 MeV for the transitions to the 3^- and 5^- states. These angular correlations display a strong peaking at backward angles, in particular for ground state transitions where about 4–5 times more counts are observed in the detectors located close to 180° than in those around 90°. They have been analyzed following the procedure reported in Sec. IV A. The results are reported in Table I.

The angular correlations measured for ground state transitions have been compared to the theoretical functions of Fig. 4, for each possible initial single-particle configuration. The theoretical curves giving the best agreement with the data are shown in Fig. 9. The angular correlation measured for excitation energies below 6.2 MeV is well reproduced by assuming that neutrons are emitted by $7/2^+$ states, due to a primary excitation of the $1g_{7/2}$ component in the $(\alpha,^3\mathrm{He})$ reaction. For the 6.6 MeV structure, a more pronounced backward yield may be observed, which is well reproduced by the theoretical angular correlation for $h_{11/2}$ emitting states, as shown in Fig. 9. On the other hand, the result of the least squares fitting procedure for the ground state decay of the 7–8 MeV excitation energy bin indicates that corresponding neutrons are mainly emitted from $g_{7/2}$ states.

Above 7 MeV, neutron decay to the 3^- state becomes energetically possible and the angular correlation measured for neutron decay of the 7.2–8 MeV excitation energy bin to the 3^- and 5^- is reasonably reproduced by the predictions for a $h_{11/2}$ state, decaying by a $d_{5/2}$ partial wave. On the other hand, the angular correlation for the decay of the 7.8–8.5 energy bin to the 5^- state can be fitted by assuming a mixing of 50% $h_{11/2}$ and 50% $k_{17/2}$ states, decaying by pure $s_{1/2}$ and $f_{7/2}$ partial waves, respectively. The corresponding theoretical angular correlations are shown in Fig. 9.

About 70% of the ^{209}Pb states excited by the $(\alpha,^3\mathrm{He})$

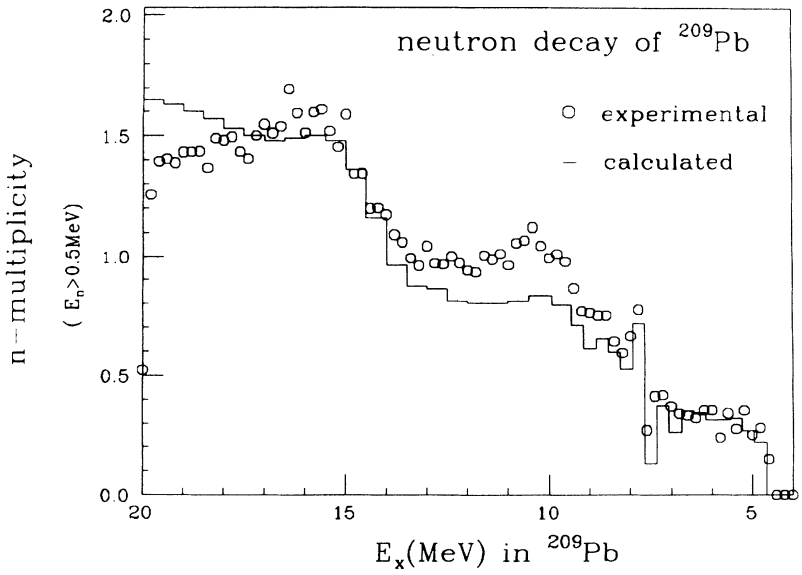

FIG. 8. Multiplicity of neutrons with energies above 0.5 MeV, as function of excitation energy in ^{209}Pb (experimental points), compared with the predictions of the statistical model (histograms).

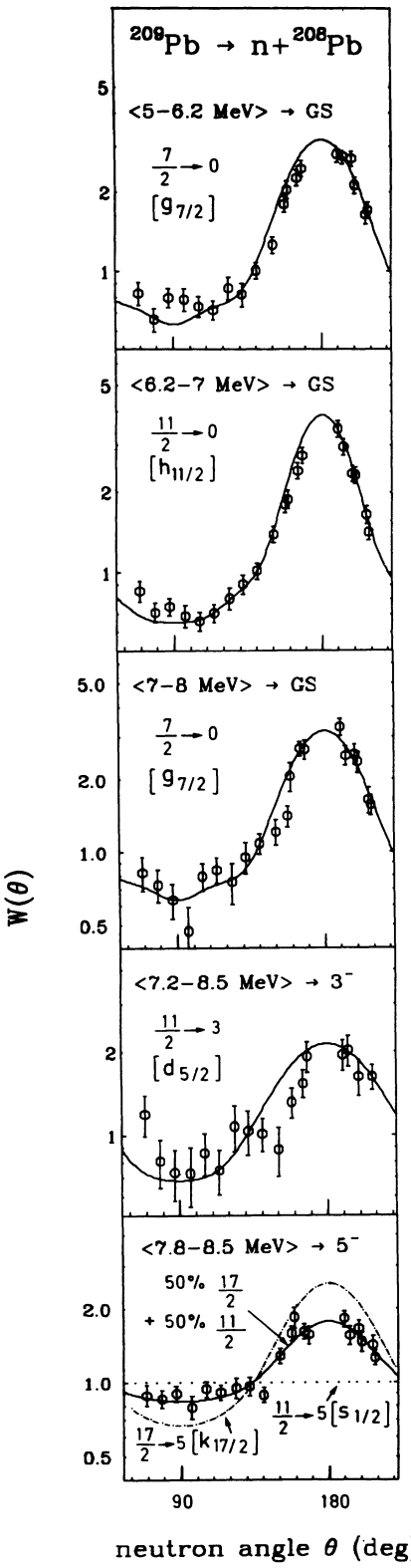

FIG. 9. Angular correlations of neutrons from different energy bins below 8.5 MeV in ^{209}Pb, compared with theoretical curves for $J_a \rightarrow J_b$ transitions. The corresponding partial waves considered in the calculations are indicated into brackets. Density matrices for initial states with J_a equal to 7/2 and 11/2 were calculated assuming (α,^{3}He) transfer to the $2g_{7/2}$ and $2h_{11/2}$ orbitals, respectively.

reaction below 7.5 MeV decay by γ-ray emission, as inferred from the measured neutron multiplicity displayed in Fig. 8. This part of the inclusive spectrum displays narrow peaks, whose energies are given in Table I. Neutron decay for these high-spin states, in particular $k_{17/2}$ components, becomes possible only above the threshold for neutron emission to the 5^- states, leading to a neutron multiplicity of about 0.7 at 8 MeV excitation energy.

The spin distributions adopted for the statistical calculations, which were displayed in Fig. 5, are in good agreement with the spin values deduced from the angular correlation analysis. The observed multiplicity provides a strong constraint on the initial spin distribution in ^{209}Pb to be used in the calculations. Below 6.5 MeV, the mixing of $l = 5$ and $l = 7$ strengths (corresponding to $2h_{11/2}$ and $1j_{13/2}$ subshells) together with the small $l \leq 4$ contribution extracted in the DWBA analysis [3] reproduces the observed multiplicity (see Fig. 8) except for the energies corresponding to the opening of the 3^- and 5^- decay channels, where threshold effects may play an important role. These calculations provide lower limits on spin values for the γ-ray emitting states, which are reported in Table I.

2. *Bump region: 8.5 MeV $\leq E_x \leq$ 12 MeV*

As shown in Fig. 7, the strongest branching ratios correspond to neutron decay to groups of states in ^{208}Pb located around 4.0 and 4.9 MeV, with predominant transitions to the 7^- and the 10^+ yrast levels, respectively. Up to 10 MeV excitation energy, one observes also a substantial decay branch to the 5^- state. The corresponding angular correlations are plotted in Fig. 10, together with those observed for the very weak transitions to the ground and 3^- state.

The angular correlations for emission to the groups of states centered at 4.0 (7^-)and 4.9 MeV (10^+) are almost isotropic. Such isotropy is expected when low (l, j) partial waves are predominant, due to the similar high-spin values of the initial and final states. On the other hand, the backward peaked angular distribution for the decay to the 5^- state is reasonably reproduced by assuming that the initial state is $k_{17/2}$, as shown in Fig. 10.

The transition to the ^{208}Pb ground state was found to be extremely weak. The measured branching ratio ($\simeq 3 \times 10^{-3}$) as well as the corresponding angular correlation displayed in Fig. 10 illustrates the high sensitivity of the EDEN multidetector array. In spite of the low statistics, one observes a backward peaking of the angular correlation, which is consistent with the prediction for the decay of a $k_{17/2}$ state, as shown in the figure. The weak transition to the 3^- state also displays an angular correlation consistent with predominant $k_{17/2}$ emitting states.

The predictions of the statistical model about the relative populations of the final states in ^{208}Pb are found to depend on the assumed spin distributions in ^{209}Pb, particularly for excitation energies below 10 MeV. In fact, the observed neutron spectra can only be reproduced by assuming that high-spin states with J_i equal to 17/2 are

TABLE I. Decay of ^{209}Pb unbound states observed below 8.5 MeV in the ^{208}Pb(α,^{3}He) reaction. Spin values for neutron emitting states are proposed on the basis of the angular correlation analysis (see text). Excitation energies and proposed limits on spin values of unbound levels or groups of levels which decay by γ-ray emission are also listed.

E_x (MeV) a	Decay	B b	J_i c	lj d	E_x (MeV)	Decay e	J_i f
⟨5–6.2⟩	$n \rightarrow$g.s.	0.30	7/2	$g_{7/2}$	4.94	γ	$\geq 11/2$
					5.49	γ	$\geq 11/2$
⟨6.2–7⟩	$n \rightarrow$g.s.	0.32	11/2	$h_{11/2}$	6.62	γ	$\geq 13/2$
⟨7–8⟩	$n \rightarrow$g.s.	0.12	7/2	$g_{7/2}$	7.10	γ	$\geq 13/2$
					7.42	γ	$\geq 13/2$
⟨7.2–8.5⟩	$n \rightarrow 3^-$	0.14	11/2	$d_{5/2}$	7.66	γ	$\geq 13/2$
⟨7.8–8.5⟩	$n \rightarrow 5^-$	0.42	11/2(50%)	$s_{1/2}$	8.30	γ	$\geq 17/2$
			17/2(50%)	$f_{7/2}$			
⟨8-8.5⟩	$n \rightarrow$g.s.	0.02					

[a]Energy bin considered in the angular correlation analysis.
[b]Branching ratio.
[c]Spin values of the emitting states, proposed on the basis of the angular correlation analysis (see text).
[d]Assumed partial wave.
[e]Excitation energies of levels or group of levels decaying by γ-ray emission. The uncertainty is estimated to be about 40 keV.
[f]The proposed limit on spin values of γ-ray emitting states is related to the inhibition of low-energy neutron emission, due to the existence of the centrifugal barrier.

predominant. In order to illustrate the sensitivity of the results to various spin assumptions, the neutron spectrum from the decay of a 0.5 MeV energy bin in the central part of the bump is compared in Fig. 11 with two different calculated spectra. In this region, results of the DWBA analysis [3] of inclusive angular distribution were consistent with a mixing of $1k_{17/2}$ and $1j_{13/2}$ states, with some contribution of $2h_{11/2}$ states. It can be seen in Fig. 11 that the predicted strength of the transition to the group of levels around 4.9 MeV (where known 8^+ and 10^+ states are located) is multiplied by a factor of about 2 when the assumed percentage of $17/2^+$ states varies from 50% (dotted line) to 80% (solid line). On the other hand, the calculated spectra depend weakly on the remaining relative percentages of $11/2^-$ and $13/2^-$ states.

Statistical spectra, obtained from the procedure outlined in Sec. IV B, and integrated over the energy bins 8.5–10 MeV and 10–12 MeV, are compared with the data in Fig. 12. The excess of cross section experimentally observed for several final levels of ^{208}Pb, especially the ground state and the 3^- and 5^- low-lying collective states, can be interpreted as resulting from nonstatistical, direct decay branches. The extraction of corresponding direct branching ratios will be presented in Sec. V C.

As shown in Fig. 8, the measured neutron multiplicity of neutrons with energy above the experimental threshold of 0.5 MeV increases from about 0.6 at 8.5 MeV to 1 at 10 MeV and is consistent with 1 above this excitation energy. The calculated multiplicity curve follows the same features, with a saturation value of about 0.8 above 10 MeV for a neutron decay branch of 1, due to missing neutrons with energy below 0.5 MeV. The origin of this discrepancy, which is larger than the possible experimental uncertainty (estimated to be about 15%), may be explained by the excess of high-energy neutrons observed experimentally.

3. *Continuum region: $E_x \geq 12$ MeV*

As shown in Fig. 8, the measured multiplicity is consistent with one well above the 11.3 MeV threshold for two-neutron emission. Such behavior is expected given the high-spin values of the ^{208}Pb unbound states populated after emission of the first neutron, which inhibit the decay to low-lying low-spin ^{207}Pb levels. The rise of the multiplicity curve with excitation energy between 13.5 and 16 MeV is related to the growing competition between one- and two-neutron emission, which occurs above the threshold energy for decay to the isomeric $13/2^+$ state at 1.6 MeV in ^{207}Pb. The rise of the neutron multiplicity is very well reproduced by the statistical calculations (see Fig. 8), assuming that the (α,^{3}He) cross section is mainly due to the excitation of initial states with spin 17/2,19/2, and 21/2, with the relative percentages taken from Ref. [20] which have been displayed in Fig. 5.

Above 16 MeV, the average multiplicity of neutrons with E_n >0.5 MeV is found to be about 1.5. This value is consistent, within error bars, with the prediction of statistical calculations, and corresponds to a predominant two-neutron emission, since undetected low-energy neutrons constitute an important part of the neutron spectra.

Provided that angular correlation effects may be neglected, the neutron-coincident spectrum of Fig. 3(b) is expected to originate from the convolution of the singles spectrum with the experimental multiplicity curve of Fig. 8. This is fully verified in the 12–20 MeV region and the bump observed at 16 MeV is related to the abrupt change in the energy dependance of the multiplicity, due to predominant two-neutron decay above this energy.

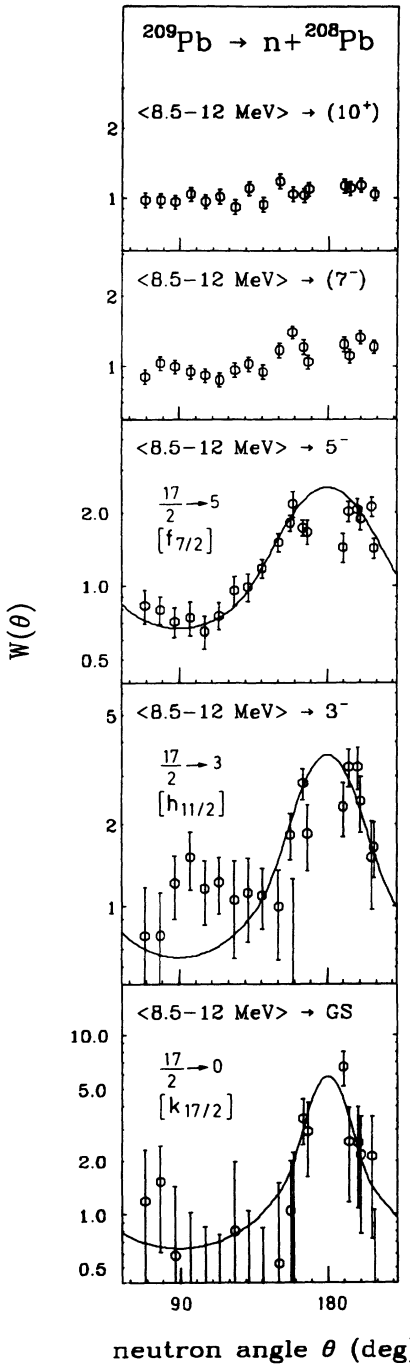

FIG. 10. Angular correlations of neutrons emitted from ^{209}Pb in the bump region. The groups of final states labeled (7^-) and (10^+) are located around 4 and 4.9 MeV in ^{208}Pb, respectively. Angular correlations to the ground state and to the 3^- and 5^- states are compared with predictions for decay of an initial state with spin 17/2.

Neutron spectra corresponding to the decay of four energy bins in ^{209}Pb between 12 and 20 MeV excitation energy are displayed in Fig. 13 as a function of the energy E_{x_b} defined in Eq. (1), and compared with the corresponding calculated spectra. The exponential shapes of the spectra are nicely reproduced by statistical calculations on a large range of neutron energies, especially above 14 MeV excitation energy.

Transitions to the groups of levels at 4.0 and 4.9 MeV, which dominate the neutron spectra below 12 MeV excitation energy in the bump region (see Fig. 12), are clearly observed up to 16 MeV. The excess of neutron decay relative to statistical predictions amounts to only about 7% of the total cross section in the 12–14 MeV region and 1.5% for the 14–16 MeV region.

Due to the logarithmic plot, the very weak one-neutron decays to the ground and 3^- states in ^{208}Pb can be observed in this whole excitation energy range. On the other hand, no significant decay to the 5^- state could be seen above 13 MeV. The angular distributions measured for the transitions to the ground and 3^- state are shown in Fig. 14. The asymmetry relative to 90° which is clearly observed for the ground state decay in Fig. 14 may be interpreted as the signature of a reaction mechanism involving elastic breakup of the α projectile. It is worth noticing that the corresponding value of $B_{a\to b}$ is smaller than 1%, showing the very weak effect of this process at the backward angles where neutrons were detected. On the other hand, the low-energy neutrons which are predominant in the decay of the ^{209}Pb continuum display a nearly isotropic angular correlation (see Fig. 14), in agreement with the predictions of the statistical model.

A detailed study of two-neutron emission was beyond the scope of this experiment. However, it was possible to extract the ^{207}Pb final energy spectrum which is displayed in Fig. 15. The energy resolution as well as the statistics are rather poor, as they have been obtained by summing the energies of two coincident neutrons and subtracting a large background of random coincident events. However, at least three structures can clearly be distinguished in this spectrum. The ^{207}Pb ground state is only weakly excited. The main structure observed at 1.6 MeV in ^{207}Pb corresponds to the feeding of the isomeric $13/2^+$ state at 1.633 MeV. The low γ-ray yield associated with the decay of the 16–20 MeV energy region, observed in Fig. 2(c), may in fact be explained by the existence of this isomeric state. The main component of the structure observed around 4 MeV has been tentatively identified with the known [23] $15/2^-$ state at 4.115±15 keV. This conclusion is supported by the observation of a 2.487 keV γ ray from the Ge(Li) detector in coincidence with ^{3}He particles feeding the region of ^{209}Pb above 16 MeV, which very probably connects the $15/2^-$ state to the $13/2^+$ isomeric state.

The two-neutron-emission component of the decay spectrum can give rise to bumps, related to the predominant excitation of a particular level in ^{207}Pb. In particular, the origin of the broad bump observed at $E_{x_b} \simeq 10$ MeV in Fig. 3 may be attributed to the feeding of the $13/2^+$ state at 1.33 MeV, as confirmed by the statistical

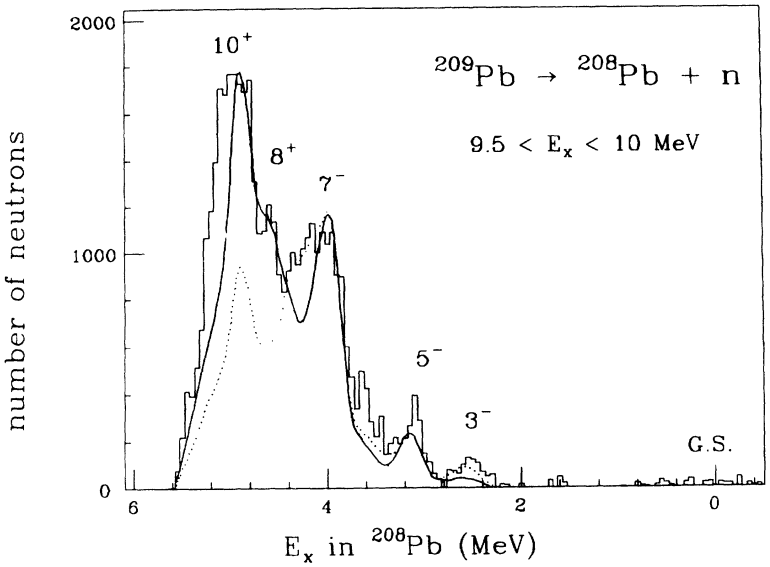

FIG. 11. Comparison of the decay spectrum of the 9.5 MeV excitation energy bin in ^{208}Pb with the results of statistical calculations. For the 9.5 MeV energy bin, the solid line corresponds to an assumed spin distribution: 80% $17/2^+$, 10% $13/2^-$, 10% $11/2^-$; the dotted line corresponds to 50% $17/2^+$, 50% $11/2^-$.

calculations.

In conclusion, the observed rise of the neutron multiplicity above 13.5 MeV, related to the opening of decay channels of two-neutron emission exciting high-spin states in ^{207}Pb, is well reproduced by the statistical model calculations. The statistical fraction of the total decay cross section which is deduced from our calculations for the [12–14 MeV] and [14–16 MeV] regions is very large, as it amounts to about 92% and 98%, respectively. Above 16 MeV, the neutron decay spectra appear to be mainly statistical, leading to the conclusion that there is an almost complete thermalization of the single-particle mode above this energy.

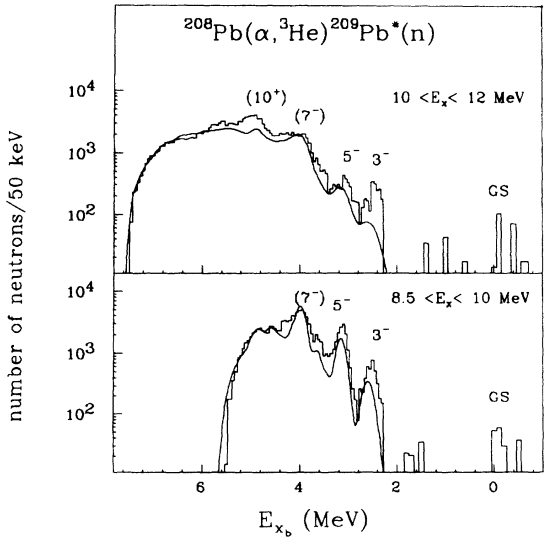

FIG. 12. Neutron spectra (histograms) from the high-spin single-particle structure observed around 10 MeV excitation energy in ^{209}Pb, compared with the predictions of the statistical model (solid lines). The channel width is 0.05 MeV, except for neutrons feeding the ground state of ^{208}Pb which are displayed using a 0.25 MeV channel width.

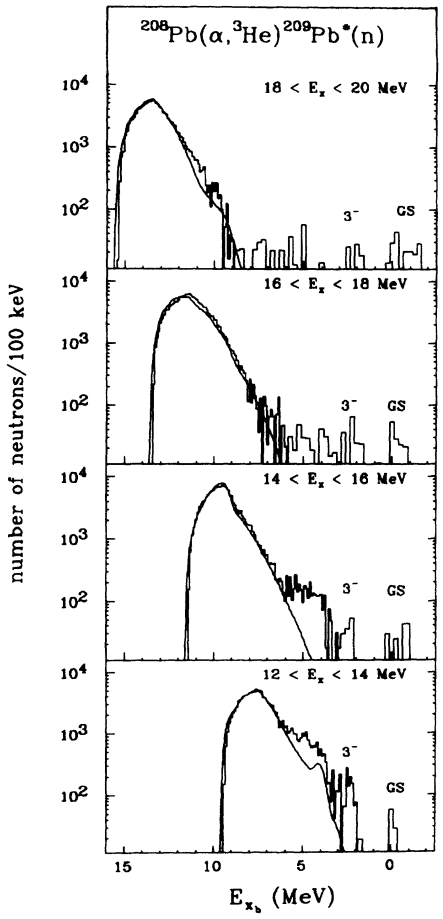

FIG. 13. Experimental neutron spectra (histograms) from four energy bins above 12 MeV in ^{209}Pb, displayed as a function of apparent excitation energy in ^{208}Pb. The channel width is 0.25 MeV for weakly populated low-lying states in ^{208}Pb corresponding to neutron energies above 8 MeV, and 0.1 MeV for higher E_{x_b} values. Corresponding spectra predicted by statistical model calculations (solid lines) are also shown for comparison.

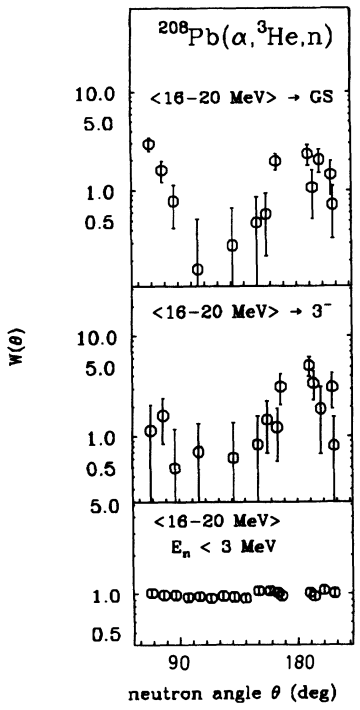

FIG. 14. Angular correlations measured for neutrons emitted by ^{209}Pb in the 16–20 MeV energy range.

B. Determination of $\Gamma^{\uparrow}/\Gamma$ branching ratios

The final states of ^{208}Pb populated in the neutron decay of ^{209}Pb have been presented in Fig. 3. Due to the good energy resolution provided by the multidetector EDEN, the peaks corresponding to the excitation of the 0^+ ground state and the 3^- and 5^- collective states are well separated. Consequently, one can extract a direct branching ratio for each of these individual states. Decay to high-spin states (7^-,8^+,10^+,...) located at higher energy and selectively populated among a high density of levels, will also be discussed and compared with statistical model predictions in order to obtain information on the role of these states in the decay of ^{209}Pb.

The dependence of statistical branching ratios $(\Gamma_n^i/\Gamma)_{calc}$ on excitation energy in the 7–12 MeV region is presented in Fig. 16 for transitions to the ground state and to the main excited levels or groups of levels of ^{208}Pb. These calculated values can be compared with the corresponding measured branching ratios, which are also displayed in the same figure. Experimental and calculated branching ratios integrated over the low-energy and high-energy parts of the 10 MeV structure are also given in Table II.

Below 7 MeV only the decay to the ground state is energetically possible, so that it is not possible to determine whether the decay is statistical or direct. In a wide excitation energy range around 10 MeV, the experimental branching ratios for the ground state, the 3^- and 5^- states, are clearly higher than the predicted ones. The branching ratio measured for the decay to the ground state is quite low but at least one order of magnitude

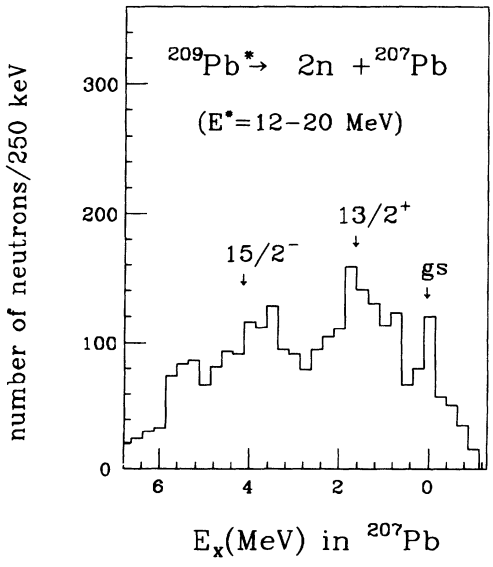

FIG. 15. Summed energy spectrum of two coincident neutrons feeding the ^{207}Pb nucleus.

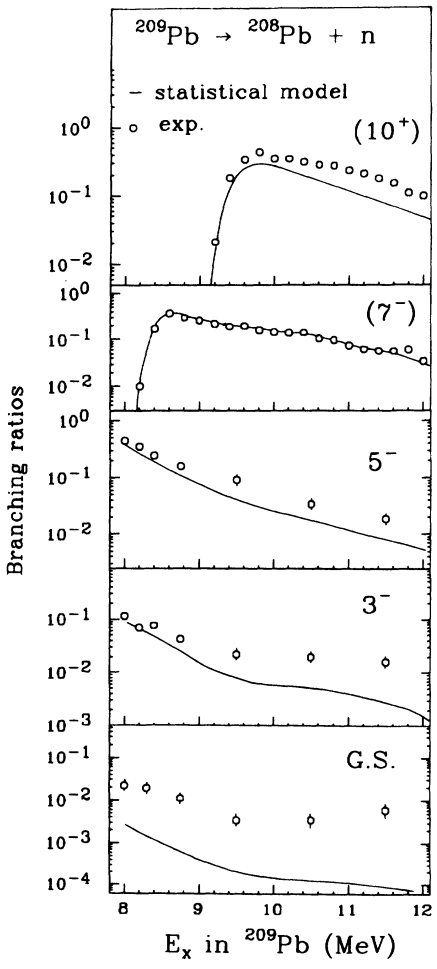

FIG. 16. Branching ratios for neutron decay to different states in ^{208}Pb, compared with the predictions of statistical calculations.

TABLE II. Direct branching ratios determined for the high-lying structure at 10 MeV in ^{209}Pb. Values of $\Gamma^{\uparrow}/\Gamma$ are extracted according to Eq. (6).

E_x (MeV)		$(\Gamma_n/\Gamma)_{expt}$ (%)	$(\Gamma_n/\Gamma)_{calc}$ (%)	$\Gamma^{\uparrow}/\Gamma$ (%)
⟨8.5–10⟩	→g.s.	0.52 ± 0.20	0.04	0.49
	→ 3$^-$	3.3 ± 0.4	1.5	2.1
	→5$^-$	12.3 ± 0.4	6.7	7.0
⟨10–12⟩	→g.s.	0.37 ± 0.12	0.01	0.36
	→ 3$^-$	1.8 ± 0.2	0.4	1.5
	→ 5$^-$	2.4 ± 0.3	1.4	1.3

larger than predicted by the statistical model. In the 8.5–10 MeV region, the experimental 5$^-$ branching ratio is higher than the one measured for the 3$^-$ state. In the 10–12 MeV region, the branching ratios for the 3$^-$ and 5$^-$ states are found experimentally to be quite comparable, whereas statistical calculations predict a larger decay branch to the 5$^-$ state. However, the experimental values are generally significantly larger than the calculated ones.

This is an important result leading to the conclusion that a sizeable amount of direct decay can be extracted and compared to theoretical predictions. The normalization factor F to be used in Eq. (6) was found to be about 0.80. The direct branching ratios $\Gamma^{\uparrow}/\Gamma$ thus deduced from Eq. (7) are reported in Table II. It is difficult to evaluate the possible error bars on these values, particularly when the statistical branching ratios are not much smaller than the experimental ones, as in the case of the 3$^-$ and 5$^-$ decay branches of the 8–9 MeV energy bin. However, one has to recall that the parameters of the present statistical model calculations were adjusted in order to maximize the statistical decay contribution. Therefore the numbers given in Table II may be considered in the worse case as a lower limit on the direct branching ratios, the higher limit being $(\Gamma_n/\Gamma)_{expt}$ if, on the contrary, the statistical contribution were negligible.

The sum of the direct branching ratios to the ground state and to the 3$^-$ and 5$^-$ states, averaged over the 8.5–12 MeV excitation energy range, amounts to 6%. This value is quite comparable to the corresponding quantity found experimentally for the direct neutron decay of the giant monopole resonance in the lead region [24].

We also extracted the branching ratio corresponding to the groups of levels around 4 MeV and 4.9 MeV, labeled (7$^-$) and (10$^+$) in Fig. 16, respectively. However, many levels are known in these energy regions in addition to the 7$^-$ state at 4.037 MeV and the 10$^+$ state at 5.010 MeV; therefore, the comparison with the predictions of microscopic structure calculations is not possible in practice. The decay to the region around the 7$^-$ state is in agreement with the predictions of the statistical model. On the contrary, the decay to the 10$^+$ region is not reproduced by the calculation (see Fig. 12 and 15), implying that there may be some direct decay to high-spin noncollective states. However, this conclusion cannot be firmly established, due to the uncertainties in the level densities in this intermediate excitation energy region.

VI. SUMMARY

The neutron decay of high-spin resonant states in ^{209}Pb excited by the (α,^{3}He) reaction has been investigated for the first time over a wide range of excitation energies with the multidetector EDEN. The unique performance of this neutron detector allowed the measurement of angular correlations, branching ratios, and neutron multiplicity with high statistics and accuracy. The dependence of the multiplicity on energy, as well as the results of the angular correlation analysis, has confirmed the high-spin character of the emitting states.

High-lying single-particle modes in ^{209}Pb, corresponding to the $2h_{11/2}$, $1j_{13/2}$, and $1k_{17/2}$ subshells and located between 8.5 and 12 MeV excitation energy, display significant direct feeding of the ground state and low-lying collective states in ^{208}Pb. The comparison of the direct branching ratios deduced from the experiment with microscopic nuclear structure calculations is underway.

On the other hand, it should be stressed that the strong population of the 10$^+$ level at 4.9 MeV and neighboring levels could not be reproduced by the present statistical calculations. It cannot be fully excluded that a better choice of the level density parameters and spin distribution in the emitting nucleus, used as input data of these calculations, would lead to a better agreement between experimental and statistical branching ratios. Otherwise, the present data may be interpreted as an evidence for direct decay branches to noncollective levels, which could act as doorway states in the damping process. It can be noticed that such decay mode is presently not included in the microscopic theory of the damping of the simple modes of excitation of the nucleus.

Above 16 MeV, the very weak population of the ground state of ^{208}Pb could be partly due to an elastic breakup process, as inferred from the angular correlation results. The present experiment clearly shows that continuum states above this energy have a decay pattern almost fully consistent with the statistical assumption, which leads to the conclusion that the degree of thermalization of the single-particle mode is close to 1 at excitation energies higher than 16 MeV in the lead region. The present data will be compared in a forthcoming paper with the results from similar experiments on ^{48}Ca, ^{90}Zr, and ^{120}Sn, which are carried out in order to establish the dependence on mass and excitation energy of the damping process of high-lying single-particle modes in nuclei.

ACKNOWLEDGMENTS

We acknowledge the operating crew of the KVI cyclotron and the physicists who helped us at different stages of the experiment. We particularly wish to thank Prof. S. Van der Werf, Prof. A. Van der Woude, and Dr. J. Van de Wiele for their support during all this work and for fruitful discussions. Dr. A. Bonaccorso and Dr. Nguyen Van Giai are also acknowledged for their continuing interest and for the communication of their theoretical predictions before publication.

[1] S. Gales, Ch. Stoyanov, and A. I. Vdovin, Phys. Rep. **166**, 127 (1988).
[2] Nguyen Van Giai and Ch. Stoyanov, Phys. Lett. B **272**, 178 (1991).
[3] C. P. Massolo, F. Azaiez, S. Galès, S. Fortier, E. Gerlic, J. Guillot, E. Hourani, and J. M. Maison, Phys. Rev. C **34**, 1256 (1986).
[4] S. Fortier, S. Galès, S. M. Austin, W. Benenson, G. M. Crawley, C. Djalali, J. S. Winfield, and G. Yoo, Phys. Rev. C **41**, 2689 (1990).
[5] I. Lhenry, Ph.D. thesis, Université Paris XI, 1991 (unpublished).
[6] H. Laurent, H. Lefort, D. Beaumel, Y. Blumenfeld, S. Fortier, S. Galès, J. Guillot, J. C. Roynette, P. Volkov, and S. Brandenburg, Nucl. Instrum. Methods A **326**, 517 (1993).
[7] A. G. Drentje, H. A. Enge, and S. B. Kowalski, Nucl. Instrum. Methods **122**, 485 (1973).
[8] J. M. Schippers, W. T. A. Borghols, and S. Y. Van der Werf, Nucl. Instrum. Methods A **247**, 467 (1986).
[9] A. E. Litherland and A. J. Ferguson, Can. J. Phys. **39**, 788 (1961).
[10] A. R. Poletti and E. K. Warburton, Phys. Rev. **137**, 595 (1967).
[11] S. Galès, S. Fortier, H. Laurent, and J. P. Schapira, Nucl. Phys. **A259**, 189 (1976).
[12] M. E. Rose, Phys. Rev. **91**, 610 (1953).
[13] J. Van de Wiele (private communication).
[14] P. D. Kunz, computer code DWUCK4 (unpublished).
[15] C. M. Vincent and H. T. Fortune, Phys. Rev. C **2**, 782 (1970).
[16] C. M. Perey and F. G. Perey, At. Data Nucl. Data Tables **17**, 1 (1976).
[17] F. Puhlofer, Nucl. Phys. **A280**, 267 (1970); M. N. Harakeh, modified version of computer code CASCADE (private communication).
[18] D. Wilmore and P. E. Hodgson, Nucl. Phys. **55**, 673 (1963).
[19] J. Rappaport *et al.*, Nucl. Phys. **A330**, 15 (1979).
[20] A. Bonaccorso (private communication).
[21] A. Bonaccorso and D. Brink, Phys. Rev. C **44**, 1559 (1991).
[22] W. Dilg, W. Schantl, H. Vonach, and M. Uhl, Nucl. Phys. **A217**, 269 (1973).
[23] M. R. Schmorak, Nucl. Data Sheets **43**, 383 (1984).
[24] S. Brandenburg *et al.*, Nucl. Phys. **A482**, 453 (1988).